IL NUOVO CIMENTO **42 C** (2019) 219
DOI 10.1393/ncc/i2019-19219-2

COMMUNICATIONS: SIF Congress 2018

First observation of $B^0_{(s)} \to J/\psi\, p\bar{p}$ decays and precise measurement of $B^0_{(s)}$ masses

E. SPADARO NORELLA(1)(2)

(1) *INFN, Sezione di Milano - Milano, Italy*
(2) *Dipartimento di Fisica, Università di Milano - Milano, Italy*

received 7 April 2019

Summary. — In this article the first observation of $B^0_{(s)} \to J/\psi\, p\bar{p}$ is reported along with the most precise $B^0_{(s)}$ mass measurements. The analysis is performed using the data sample collected by LHCb during 2011–2016, corresponding to an integrated luminosity of 5.2 fb^{-1}. The $B^0_{(s)} \to J/\psi\, p\bar{p}$ decays are suppressed due to the OZI and Cabibbo rules, as well as due to the limited available phase space. The branching fractions are measured to be $\mathcal{B}(B^0 \to J/\psi\, p\bar{p}) = (4.51 \pm 0.40\ (\text{stat}) \pm 0.44\ (\text{syst})) \times 10^{-7}$ and $\mathcal{B}(B^0_s \to J/\psi\, p\bar{p}) = (3.58 \pm 0.19\ (\text{stat}) \pm 0.39\ (\text{syst})) \times 10^{-6}$. The B^0_s branching fraction is two order of magnitude higher than a naïve expectation of $O(10^{-9})$. The suppression can be lifted by the existence of pentaquarks and glueballs in the $J/\psi\, p$ and $p\bar{p}$ system, respectively. In addition, due to the limited available phase space, the most precise mass measurements are permitted. The measured value of the B^0 mass is 5279.74 ± 0.30 (stat) $\pm$ 0.10 (syst) MeV, and that of the B^0_s mass is 5366.85 ± 0.19 (stat) $\pm$ 0.13 (syst) MeV.

1. – Introduction

Decays of B mesons to final states containing baryons have a long and interesting history, starting with the first observation of the baryonic $B^+ \to \Lambda_c^+ \bar{p}\pi^-$ decay at CLEO [1]. Numerous studies of B^+ and B^0 baryonic decays were performed at the B-factories. The branching fractions for multi-body are typically larger than the two-body final states. It was only with the advent of data from LHCb that the first two-body baryonic mode $B^+ \to p\overline{\Lambda}(1520)$ was observed [2]. More recently, LHCb has also reported the first observations of baryonic decays for the $B^0_s \to p\Lambda_c^+ K^-$ [3] and $B_c^+ \to J/\psi\, p\bar{p}\pi^+$ [4] mesons.

The decays of $B^0_{(s)} \to J/\psi\, p\bar{p}$ are interesting for several reasons. First of all, they are suppressed compared to the mesonic $B^0_s \to J/\psi\, K^+K^-$ or $B^0 \to J/\psi\, \pi^+\pi^-$ decays due to the much smaller available phase space. Further suppression comes from OZI suppression for B^0_s and Cabibbo suppression for the B^0 because of the CKM matrix element $|V_{cd}|$. The naïve estimated branching fraction for the B^0_s decay is of the order of 10^{-9} [5]. However, the presence of an intermediate state can enhance the measured branching-fraction value. A preliminary analysis performed by LHCb with data corresponding to

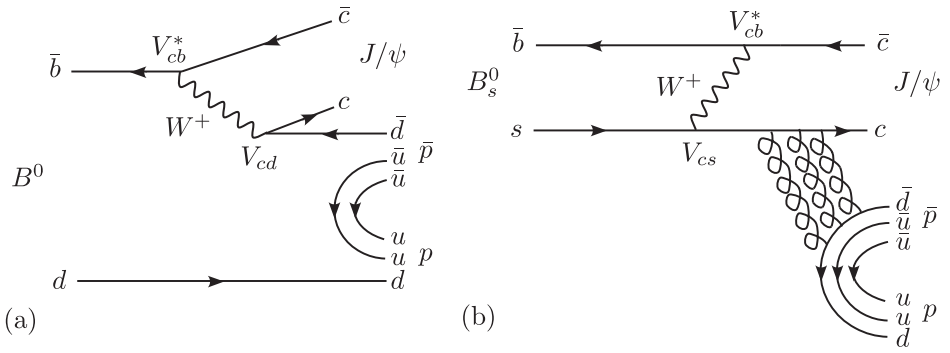

Fig. 1. – Leading-order Feynman diagrams for B^0 (a) and B_s^0 (b) decays.

1 fb^{-1} showed discrepancy with the expectation for the B_s^0 mode of around 2 order of magnitude [6]. However, only an excess was observed with a statistical significance of around 2.8 σ for the B_s^0 mode. Figure 1 shows the leading-order Feynman diagrams for the two decays. For the B_s^0 mode a possible intermediate glueball resonance $f_J(2220)$ decaying to $p\bar{p}$ final state can come in, as predicted by Hsiao [5]. This is the baryonic equivalent of $B_s^0 \to J/\psi\, f_0(980)(\to \pi^+\pi^-)$ that has been studied at LHCb [7] earlier. Similarly, the $B^0 \to J/\psi\, p\bar{p}$ mode is the baryonic version of $B^0 \to J/\psi\, \pi^+\pi^-$ that has also been studied by LHCb [8] previously. Being a $b \to d$ transition, this mode is sensitive to the so-called "penguin pollution" in determination of the angle β [8], since both the tree and penguin components in fig. 1(a) are comparable.

Another interesting prospect for these modes is the possibility of pentaquarks occuring in the $J/\psi\, p$ or $J/\psi\, \bar{p}$ invariant masses. Since the B^0 mode has a quite restricted phase space, this is more than a possibility for the B_s^0 mode. In the analysis of $\Lambda_b \to J/\psi\, pK^-$, LHCb observed [9] two resonances consistent with pentaquarks, of masses $\sim$4380 and $\sim$4450 MeV, widths $\sim$205 MeV and $\sim$39 MeV and spins $J = \frac{3}{2}$ and $J = \frac{5}{2}$, respectively. Recently LHCb published new results [10] on the same decay channel revealing the existence of a new narrower peak at mass 4312 MeV and the presence of a more complex structure corresponding to the peak at 4450 MeV. This intermediate state is split into two peaks at masses around 4440 MeV and 4457 MeV, respectively. The $B_{(s)}^0 \to J/\psi\, p\bar{p}$ decays are particularly attractive for the ground state (spin $\frac{1}{2}$) pentaquarks, while the broad $P_c^+(4380)$ is directly accessible for the B_s^0 mode. A full amplititude analysis would be needed to search for pentaquark and glueball existence.

In this article, the first observation of $B_{(s)}^0 \to J/\psi\, p\bar{p}$ decays is presented along with the mass measurements of B_s^0 and B^0 mesons [11]. The analysis is performed using the data collected by LHCb in 2011–2016 corresponding to an integrated luminosity of 5.2 fb^{-1}. The small B_s^0 breakup momentum of $Q \sim 394$ MeV in the $B_s^0 \to J/\psi\, p\bar{p}$ decay allows for the most precise measurement of the B_s^0 mass. The precise B^0 mass measurement is also reported. As a control mode, the well-measured $B_s^0 \to J/\psi\, \phi(\to K^+K^-)$ decay is used, similar in topology to the signal mode.

2. – Detector

The LHCb detector [12, 13] is a single-arm forward spectrometer covering the pseudorapidity range $2 < \eta < 5$, designed for the study of particles containing b or c quarks. The detector includes a high-precision tracking system consisting of a silicon-

strip vertex detector surrounding the pp interaction region [14], a large-area silicon-strip detector located upstream of a dipole magnet with a bending power of about 4 Tm, and three stations of silicon-strip detectors and straw drift tubes [15] placed downstream of the magnet. The tracking system provides a measurement of momentum, p, of charged particles with a relative uncertainty that varies from 0.5% at low momentum to 1.0% at 200 GeV. The minimum distance of a track to a primary vertex (PV), the impact parameter (IP), is measured with a resolution of $(15 + 29/p_{\rm T})\,\mu$m, where $p_{\rm T}$ is the component of the momentum transverse to the beam, in GeV. Different types of charged hadrons are distinguished using information from two ring-imaging Cherenkov detectors [16]. Photons, electrons and hadrons are identified by a calorimeter system consisting of scintillating-pad and preshower detectors, an electromagnetic calorimeter and a hadronic calorimeter. Muons are identified by a system composed of alternating layers of iron and multiwire proportional chambers [17]. The online event selection is performed by a trigger [18], comprising a hardware stage based on information from the calorimeter and muon systems, followed by a software stage that applies a full event reconstruction. The software trigger selects events that contain dimuon tracks originating from a secondary decay vertex, J/ψ candidate, detached from the primary pp collision point.

The properties of the signal and control channels are studied exploiting simulation samples based on Monte Carlo (MC) techniques. The pp collisions are generated using Pythia [19] with a specific LHCb configuration [20]. Decays of hadronic particles are described by EvtGen [21], in which final-state radiation is generated using Photos [22]. The $B^0_s \to J/\psi\,\phi$-mode simulations are generated according to a decay model studied in ref. [23], while the signal $B^0_{(s)} \to J/\psi\, p\bar{p}$ modes are generated following a uniform distribution in phase-space. The interaction of the generated particles with the detector, and its response are implemented using the Geant4 toolkit [24] as described in ref. [25].

3. – Selection

In order to achieve a good event selection, the excellent vertexing and charged particle identification (PID) of the LHCb detector are exploited. Signal candidates are built from two oppositely charged tracks, identified as muons and originating from a J/ψ vertex displaced from the PV. Another pair of charged tracks consistent with p and $\bar{p}$ is combined with the dimuon tracks to form a $B^0_{(s)}$ candidate with the entire decay topology constrained by a kinematic fit. The dimuon invariant mass is constrained to be equal to the nominal J/ψ mass [26]. For the $B^0_s \to J/\psi\,\phi$ control mode a similar procedure is followed, replacing the $p\bar{p}$ combination with a pair of charged tracks associated to K^+K^- candidates, satisfying $|m(K^+K^-) - 1020| < 5\,$MeV, to select the $\phi(1020)$ resonance region [26]. All charged tracks are required to be of good quality, with $p_{\rm T} > 300\,$MeV ($p_{\rm T} > 550\,$MeV) for p or K (μ). At this stage, the background is composed by combinatorial tracks, composed by other hadrons (π and K) misidentified as protons.

In order to achieve a good background suppression, the selection is optimized with multivariate techniques based on Boosted Decision Tree (BDT) alghorithms [27]. Before the training, some of the MC distributions have to be corrected to be representative of real data. These corrections concern kinematic distributions of the B^0 meson, like p, $p_{\rm T}$ and the number of tracks per event. These variables are not well reproduced by Pythia because of the b hadronization in B^0 meson. A weight is computed for each signal candidate, in the space of the interesting variables, as the difference between simulation and background-substracted data of the $B^0_s \to J/\psi\,\phi$ control mode.

The background-substracted data is obtained using the *sPlot* technique [28]. The weights are derived exploiting a multi-dimentional technique based on a boosted decision tree to choose the regions more suitable for weighting. These weights are then applied to both the $B^0_{(s)} \to J/\psi p\bar{p}$ signal modes and the $B^0_s \to J/\psi\,\phi$ control mode simulations. The second correction concerns the PID variables. In this analysis, PID is exploited to obtain a clean sample of signal B^0_s events by discrimating signal from combinatorial background. In order to improve the agreement, the distribution for each PID variable is resampled using calibration samples extracted directly from data. The samples are obtained from $\Lambda_c^+ \to pK^-\pi^+$ and $D^{*+} \to D^0(\to K^-\pi^+)\pi^+$ decays and the correction is performed taking into account the dependence of each track from p, $p_{\rm T}$ and the global number of tracks in the event. Systematic uncertainties are assigned to both the methods. After the application of corrections, the selection is optimized using BDT in two stages in order to guarantee a more powerful background rejection. In the first stage, the BDT 1 classifier is trained using the high-statistics $B^0_s \to J/\psi\,\phi$ control mode as signal proxy, and employs only kinematic variables whose distributions are similar between the signal and the control mode. These include the p, $p_{\rm T}$, and $\chi^2_{\rm IP}$ of the B^0_s (χ^2 difference adding/removing final tracks to the fit on the associated PV), the χ^2 probability from a kinematic fit [29] to the decay topology, and the IP distances from the PV for the two muons. The purpose of BDT 1 is to provide a pre-selection employing a multivariate classifier sensitive to correlations among the kinematic variables, instead of rectangular selection requirements.

To choose the BDT 1 working point in an optimal but unbiased fashion, the $B^0_s \to J/\psi p\bar{p}$ signal significance, $\mathcal{S}/\sqrt{\mathcal{S}+\mathcal{B}}$, is required to just exceed 5. This choice is made to guarantee a preliminary selection that will be optimized only in the second stage. The background yield, $\mathcal{B}$, is estimated from a fit to the $B^0_{(s)} \to J/\psi p\bar{p}$ data prior to any BDT selection requirement and the signal yield, $\mathcal{S}$, is obtained from the $B^0_s \to J/\psi p\bar{p}$ branching fraction quoted in ref. [6], multiplied by the signal efficiency obtained from simulation.

In the final selection stage, the hadron PID information from the RICH detector system is considered in a second classifier, BDT 2, in order to distinguish among hadrons. The BDT 2 also includes the p, $p_{\rm T}$ and $\chi^2_{\rm IP}$ of the protons as training variables. The $B^0_s \to J/\psi p\bar{p}$ simulation is used as signal sample, while the events in data with $m(J/\psi p\bar{p}) \in [5450, 5500]\,\text{MeV}$ are used as training for the background. The optimal BDT 2 selection criterion is chosen by maximising the significance, with the initial signal and background yields extracted from a fit to the $m(J/\psi p\bar{p})$ distribution after the BDT 1 selection.

The control mode selection is performed using a single BDT classifier, which includes the same kinematic variables as in BDT 1 with the addition of the PID variables for the kaons.

After the application of the selection cuts, a maximum likelihood fit is performed on the $m(J/\psi p\bar{p})$ invariant-mass distribution in the range $[5220,\ 5420]\,\text{MeV}$. The fit model is composed by two Crystal-Ball functions [30] for the signal and a first order polynomial for the background. The invariant-mass plot and the results for the yields and masses are reported in fig. 2 and in table I. The significance of both the peaks is higher than 10σ. The average selection efficiency evaluated on simulation after the reconstruction, the trigger and the selection cut is around 1%. In fig. 3, the $m(J/\psi K^+K^-)$ invariant-mass distribution for the $B^0_s \to J/\psi\,\phi$ control mode is reported after the entire selection. The distribution is fitted with a similar lineshape for the signal and an exponential function for the background. The final yield is 136808 ± 402 number of events.

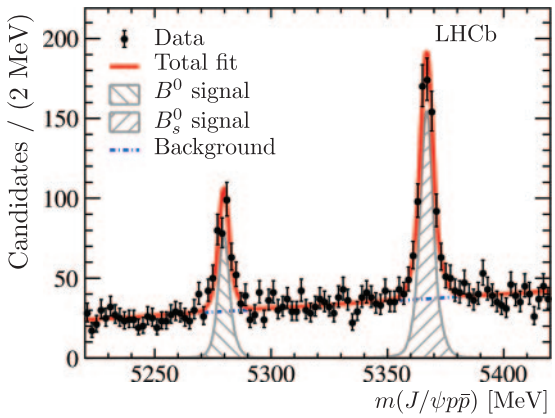

Fig. 2. – Fit to the invariant mass distribution of the $B^0_{(s)} \to J/\psi\, p\bar{p}$ signal mode.

4. – Efficiency

In order to perform a branching fraction measurement, the efficiency of the overall selection needs to be correctly evaluated for both the signal and the control mode. The simulated physics model for the control mode takes already into account the correct decay dynamics. For this reason the efficiency is averaged over the phase space. While for the signal modes, since the physics model is not known *a priori*, an efficiency parameterization is derived from simulation as a function of the kinematic variables in the event topology. An event-by-event correction is then applied to the data. The efficiency is parameterized as the product of Legendre polynomials

$$\varepsilon(\vec{\varphi}) = \sum_{i,j,k,l} c_{i,j,k,l}\; P(\cos\theta_\ell, i) P(\cos\theta_h, j) P(\chi', k) P(m'_{p\bar{p}}, l),$$

where $P(x, n)$ is a Legendre polynomial of order n in $x \in (-1, 1]$. These polynomials depend on the four kinematic variables that describe the phase space element: $m_{p\bar{p}}, \theta_\ell, \theta_h, \chi$. They are composed by the invariant mass of $p\bar{p}$, two helicity angles of the hadron and lepton in the rest frame of the decaying particle and one azimuthal angle between the two decaying planes as illustrated in fig. 4.

The phase space is defined as: $\vec{\varphi} \equiv \{m'_{p\bar{p}}, \cos\theta_\ell, \cos\theta_h, \chi'\}$, where $m'_{p\bar{p}}$ and χ' are then normalized such that all four variables in $\vec{\varphi}$ lie in the range $(-1, 1]$. A good parametrization is found for polynomials with order $\{3, 7, 7, 5\}$ for $\{m'_{p\bar{p}}, \cos\theta_\ell, \cos\theta_h, \chi'\}$, respec-

TABLE I. – *Signal yields and mass values obtained from the fit to data for B^0 and B^0_s decays.*

Mode	Yield	$B^0_{(s)}$ mass (MeV)
$B^0_s \to J/\psi\, p\bar{p}$	609 ± 31	5366.85 ± 0.19
$B^0 \to J/\psi\, p\bar{p}$	256 ± 22	5279.74 ± 0.30

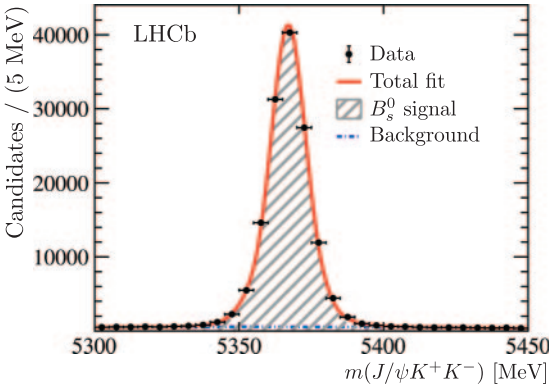

Fig. 3. – Fit to the invariant mass distribution of the $B_s^0 \to J/\psi\,\phi$ control mode.

tively. Simulation samples are used where $B^0_{(s)} \to J/\psi\, p\bar{p}$ events are generated uniformly in phase space. The coefficients, $c_{h,i,j,k,l}$, are determined from the simulation using the orthogonality of Legendre polynomials

$$c_{i,j,k,l} = C \sum_{n=0}^{N_{\rm recon}} \left(\frac{2i+1}{2}\right)\left(\frac{2j+1}{2}\right)\left(\frac{2k+1}{2}\right)\left(\frac{2l+1}{2}\right) \times P(\cos\theta_\ell, i) P(\cos\theta_h, j) P(\chi', k) P(m', l).$$

The sum is over the reconstructed events in the simulation sample after all selection criteria. The correct normalization is given by the prefactor C. For a given data event, the efficiency, $\varepsilon(\vec{\varphi})$, is computed according to the parameterization and a weight is assigned, equal to the inverse of the efficiency, $1/\varepsilon(\vec{\varphi})$.

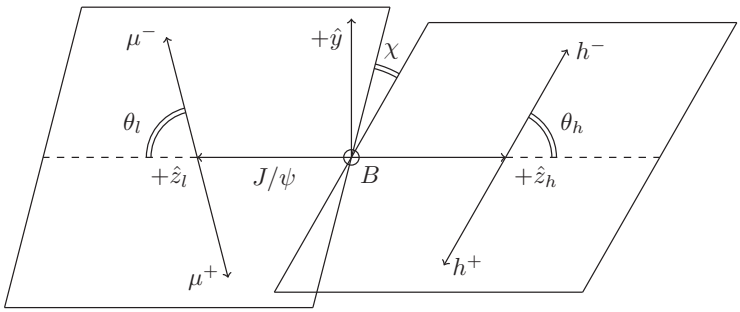

Fig. 4. – The three angular variables $\{\theta_\ell, \theta_h, \chi\}$ for the decay $B \to J/\psi(\to \mu^+\mu^-)h^+h^-$, where $h \in \{p, K\}$. The dihadron and dilepton coordinate systems lie back-to-back with a common vertical $\hat{y}$ axis. The angle between the decay planes is $\chi \in (-\pi, \pi]$, while the two helicity angles, θ_h and θ_ℓ, are defined in the dihadron and dilepton rest frames, respectively.

5. – Systematic uncertainties

Since the $B^0_s \to J/\psi\,\phi$ control mode has very similar topology to the signal mode, most of the systematic uncertainties cancel in the ratio of branching fractions. The most important systematic effects are related to the PID and the tracking efficiency. To account for the PID uncertainty, different calibration samples, based on $\Lambda \to pK^-$ decays, are used to correct the PID distributions. The systematic uncertainty is assigned as the difference between the two PID resampling methods. The second uncertainty concerns the tracking efficiency since the description provided by the simulation of the hadronic interactions with the detector material is less accurate for baryons than it is for mesons. Following ref. [31], a systematic uncertainty of 4% is assigned to protons and of 1.1% to kaons. For evaluating the systematics, the nominal tracking efficiency of each track is varied within the systematic uncertainty, following a Gaussian distribution, in a correlated way between different tracks. The resulting overall uncertainty is 5%.

Other effects include imperfections on the choice of the fit model and the weighting procedure. For the fit model systematics, 1000 mass-spectra samples are generated according to the reference fit and refitted using an alternative model composed by three Gaussian functions for the signal and an exponential function for the background. The pull distribution of the yields is assigned as a systematic uncertainty. In addition, the weighting procedure is based on the assumption that the difference between data and simulation is similar for different $B^0_{(s)} \to J/\psi\, h^+h'^-$ decay modes. As a consequence, to validate the assumption, another control mode, $B^0 \to J/\psi\, K^-\pi^+$, is used to compute the weights and the difference between the weights is assigned as a systematic uncertainty. Other smaller effects are related to trigger efficiency and the presence of more than one candidate per event. The overall systematic uncertainties contain also the uncertainty on the normalization and on the ratio f_s/f_d, which is the ratio of the hadronization probabilities of b-quark into B^0_s and B^0 mesons. This last contribution is considered for the B^0_s mode in both Run1 and in Run2, while for B^0 there is a 4.3% uncertainty in Run 2 due to the additional energy-dependent correction on f_s/f_d discussed below. The overall contributions are added in quadrature resulting in 9.4(10.1)% and 11.1(10.7)% in Run 1 (Run 2) for $\mathcal{B}(B^0 \to J/\psi\, p\bar{p})$ and for $\mathcal{B}(B^0_s \to J/\psi\, p\bar{p})$, respectively. Each contribution is summarized in table II.

6. – Branching fraction measurements

The branching fractions are measured with respect to the $B^0_s \to J/\psi\,\phi(\to K^+K^-)$ control mode as follows:

$$\frac{\mathcal{B}(B^0 \to J/\psi\, p\bar{p})}{\mathcal{B}(B^0_s \to J/\psi\,\phi(\to K^+K^-)) \times f_s/f_d} = \frac{N^{\rm corr}_{B^0\to J/\psi\, p\bar{p}}}{N^{\rm corr}_{B^0_s\to J/\psi\, K^+K^-}},$$

$$\frac{\mathcal{B}(B^0_s \to J/\psi\, p\bar{p})}{\mathcal{B}(B^0_s \to J/\psi\,\phi(\to K^+K^-))} = \frac{N^{\rm corr}_{B^0_s\to J/\psi\, p\bar{p}}}{N^{\rm corr}_{B^0_s\to J/\psi\, K^+K^-}},$$

where $N^{\rm corr}$ denotes efficiency-corrected signal yields. The final combination of branching ratios is taken as a weighted mean between Run 1 and Run 2 considering the systematic

TABLE II. – *Systematic uncertainties on the $B^0_{(s)} \to J/\psi p\bar{p}$ branching fractions for Run 1 and Run 2. The total uncertainties on the branching fraction ratios (BFR) are the sum in quadrature of the systematic uncertainties. The normalization and the uncertainties on the ratio f_s/f_d are taken from external measurements and are included in the absolute branching fractions ($\mathcal{B}$).*

	$\mathcal{B}(B^0 \to J/\psi p\bar{p})$	$\mathcal{B}(B^0_s \to J/\psi p\bar{p})$
	Run 1 (Run 2)	Run 1 (Run 2)
Fit model	1.0 (0.5)%	1.0 (0.9)%
Detector resolution	0.6 (0.5)%	0.4 (0.6)%
PID efficiency	5.0 (4.0)%	5.0 (4.0)%
Trigger	1.0 (1.0)%	1.0 (1.0)%
Tracking	5.0 (5.0)%	5.0 (5.0)%
Simulation weighting	0.4 (0.4)%	0.3 (0.3)%
Multiple candidates	0.1 (0.1)%	0.1 (0.1)%
Total on BFR	7.2 (6.5)%	7.2 (6.6)%
Normalization	6.1 (6.1)%	6.1 (6.1)%
f_s/f_d	– (4.3)%	5.8 (5.8)%
Total on $\mathcal{B}$	9.4 (10.1)%	11.1 (10.7)%

uncertainty to be fully correlated

$$\frac{\mathcal{B}(B^0 \to J/\psi p\bar{p})}{\mathcal{B}(B^0_s \to J/\psi\,\phi(\to K^+K^-)) \times f_s/f_d} = (0.329 \pm 0.029\ (\text{stat})) \pm 0.022\ (\text{syst})) \times 10^{-2}, \tag{4a}$$

$$\frac{\mathcal{B}(B^0_s \to J/\psi p\bar{p})}{\mathcal{B}(B^0_s \to J/\psi\,\phi(\to K^+K^-))} = (0.706 \pm 0.037\ (\text{stat}) \pm 0.048(\text{syst})) \times 10^{-2}, \tag{4b}$$

where the first uncertainty is statistical and the second is systematic. For the normalization, the values $\mathcal{B}(B^0_s \to J/\psi\,\phi(\to K^+K^-)) \times f_s/f_d = (1.314 \pm 0.016 \pm 0.079) \times 10^{-4}$ [32] and $f_s/f_d = 0.259 \pm 0.015$ [33] are assumed for Run 1, while for Run 2 the fragmentation ratio has been multiplied by an additional scale factor of 1.068 ± 0.046 [34], to take into account the dependence to the center of mass energy.

The absolute branching ratios are then combined to give

$$\mathcal{B}(B^0 \to J/\psi p\bar{p}) = (4.51 \pm 0.40\ (\text{stat}) \pm 0.44\ (\text{syst})) \times 10^{-7}, \tag{5a}$$

$$\mathcal{B}(B^0_s \to J/\psi p\bar{p}) = (3.58 \pm 0.19\ (\text{stat}) \pm 0.39\ (\text{syst})) \times 10^{-6}, \tag{5b}$$

where the first uncertainty is statistical and the second one is systematic.

7. – Mass measurements

The small Q-values of the $B^0_{(s)} \to J/\psi p\bar{p}$ decays allow for the most precise single measurements of the B^0 and B^0_s masses. The sources of systematic uncertainties include imperfections in the magnetic field mapping, uncertainties of particle interactions with

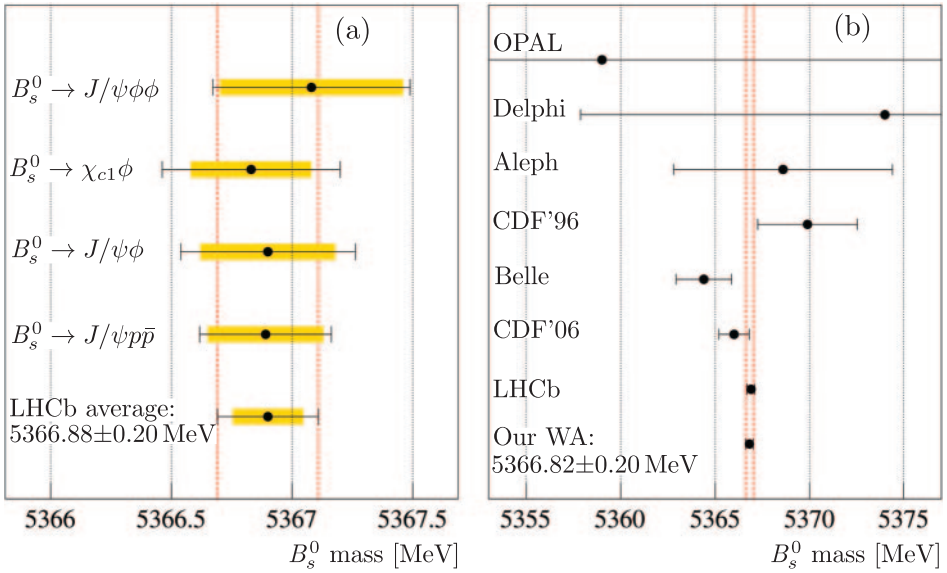

Fig. 5. – Measurements of B^0_s mass from (a) various B^0_s decay modes in LHCb [35-37], (b) world average (WA) including the present result [26].

the detector material, and the choice of the signal model. The final results are $5279.74 \pm 0.30\,(\text{stat}) \pm 0.10\,(\text{syst})$ MeV for the B^0 mass, and $5366.85 \pm 0.19\,(\text{stat}) \pm 0.13\,(\text{syst})$ MeV for the B^0_s mass. A summary of the various B^0_s mass measurements is depicted in fig. 5, where the combination of LHCb measurements is obtained considering only the systematic uncertainties derived with the same methods to be correlated.

8. – Conclusions

In summary, the first observation of the $B^0 \to J/\psi\, p\bar{p}$ and $B^0_s \to J/\psi\, p\bar{p}$ decays is reported with very high significance. The measured branching fraction for $B^0 \to J/\psi\, p\bar{p}$ is in agreement with theoretical expectations [5] while that for $B^0_s \to J/\psi\, p\bar{p}$ is enhanced by two orders of magnitude with respect to predictions. More data will allow for a full Dalitz plot analysis for glueball and pentaquark searches. The world's best single measurements of the B^0 and B^0_s masses are also obtained in this analysis.

* * *

The author acknowledges funding from Fondazione Fratelli Confalonieri, Milano.

REFERENCES

[1] CLEO Collaboration (Fu X. *et al.*), *Phys. Rev. Lett.*, **79** (1997) 3125.
[2] LHCb Collaboration (Aaij Roel *et al.*), *Phys. Rev. Lett.*, **113** (2014) 14141801.
[3] LHCb Collaboration (Aaij R. *et al.*), *First observation of a baryonic B^0_s decay*, CONF-2016-016 (2016).
[4] LHCb Collaboration (Aaij R. *et al.*), *Phys. Rev. Lett.*, **113** (2014) 15152003.
[5] Hsiao Y. K. and Geng C. Q., *Eur. Phys. J. C*, **75** (2015) 101.
[6] LHCb Collaboration (Aaij R. *et al.*), *JHEP*, **09** (2013) 006.

[7] LHCb Collaboration (Aaij R. *et al.*), *Phys. Rev. D*, **86** (2012) 052006.
[8] LHCb Collaboration (Aaij R. *et al.*), *Phys. Rev. D*, **87** (2013) 5052001.
[9] LHCb Collaboration (Aaij R. *et al.*), *Phys. Rev. Lett.*, **115** (2015) 072001.
[10] LHCb Collaboration, *Phys. Rev. Lett.*, **122** (2019) 222001.
[11] LHCb Collaboration (Aaij R. *et al.*), *Phys. Rev. Lett.*, **122** (2019) 191804.
[12] LHCb Collaboration (Alves A. A. jr. *et al.*), *JINST*, **3** (2008) S08005.
[13] LHCb Collaboration (Aaij R. *et al.*), *Int. J. Mod. Phys. A*, **30** (2015) 1530022.
[14] LHCb Collaboration (Aaij R. *et al.*), *JINST*, **9** (2014) P09007.
[15] Arink R. *et al.*, *JINST*, **9** (2014) P01002.
[16] Adinolfi M. *et al.*, *Eur. Phys. J. C*, **73** (2013) 2431.
[17] Alves A. A. jr. *et al.*, *JINST*, **8** (2013) P02022.
[18] Aaij R. *et al.*, *JINST*, **8** (2013) P04022.
[19] Sjöstrand Torbjörn, Mrenna Stephen and Skands Peter, *JHEP*, **05** (2006) 026.
[20] Belyaev I. *et al.*, *J. Phys. Conf. Ser.*, **331** (2011) 032047.
[21] Lange, D. J., *Nucl. Instrum. Methods A*, **462** (2001) 152.
[22] Golonka Piotr and Was Zbigniew, *Eur. Phys. J. C*, **45** (2006) 97.
[23] LHCb Collaboration (Aaij *et al.*), *Phys. Rev. Lett.*, **114** (2015) 4041801.
[24] Geant4 collaboration (Allison John, Amako K., Apostolakis J., Araujo H., Dubois P. A. *et al.*), *IEEE Trans. Nucl. Sci.*, **53** (2006) 270.
[25] Clemencic M. *et al.*, *J. Phys. Conf. Ser.*, **331** (2011) 032023.
[26] Particle Data Group (Patrignani C. *et al.*), *Chin. Phys. C*, **40** (2016) 100001.
[27] Breiman L., Friedman J. H., Olshen R. A. and Stone C. J., *Classification and Regression Trees*, (Wadsworth International Group) 1984.
[28] Pivk Muriel and Le Diberder Francois R., *Nucl. Instrum. Methods A*, **555** (2005) 356.
[29] Hulsbergen Wouter D., *Nucl. Instrum. Methods A*, **552** (2005) 566.
[30] Oreglia M., *A Study of the Reactions* $\psi' \to \gamma\gamma\psi$, SLAC, PhD Thesis (1980).
[31] LHCb Collaboration (Aaij R. *et al.*), *JHEP*, **04** (2017) 162.
[32] LHCb Collaboration (Aaij R. *et al.*), *Phys. Rev. D*, **87** (2013) 072004.
[33] LHCb Collaboration, *Updated average* f_s/f_d *b-hadron production fraction ratio for 7 TeV pp collisions*, CONF-2013-011, Jul. 2013.
[34] LHCb Collaboration (Aaij R. *et al.*), *Phys. Rev. Lett.*, **118** (2017) 191801.
[35] LHCb Collaboration (Aaij R. *et al.*), *JHEP*, **03** (2016) 040.
[36] LHCb Collaboration (Aaij R. *et al.*), *JHEP*, **08** (2018) 191.
[37] LHCb Collaboration (Aaij R. *et al.*), *Phys. Lett. B*, **708** (2012) 241.